

Contents

1 Fundamentals 1

1.1	EUV and X-ray Radiation	1
1.2	Interaction of EUV and X-ray Radiation With Matter	2
1.2.1	Elastic Scattering	4
1.2.2	Absorption and Fluorescence Radiation	6
1.3	Specular Reflectance from Surfaces and Interfaces in Multilayer Systems	7
1.4	Diffuse Scattering in Layered Systems	11
1.4.1	The DWBA Scattering Cross Section	12
1.5	Grazing-incidence X-ray Fluorescence	17

*un 1 überprüfen
=> Ur 9*

References 21

Abbreviations

DWBA distorted-wave Born approximation.

EUV extreme ultraviolet.

eV electron volt.

PSD power spectral density.

r.m.s. root mean square.

XRF X-ray fluorescence.

XSW X-ray standing wave.

Symbols

α_f	scattering angle defined from the surface normal.
α_i	angle of incidence defined from the surface normal.
c	speed of light in vacuum $c = 1/\sqrt{\epsilon_0 \mu_0}$.
ϵ_0	vacuum permittivity or electric constant.
h	Planck's constant, $h = 4.135667662(25) \times 10^{-15}$ eV s.
\vec{k}	wave vector; the wave number is $ \vec{k} = k_0 = 2\pi/\lambda$.
k_0	modulus of the wave vector in vacuum (wave number) $k_0 = \omega/c = 2\pi/\lambda$.
λ	wavelength.
μ_0	vacuum permeability or magnetic constant.
n	complex index of refraction, $n = \delta + i\beta$.
ω	frequency.
\vec{q}	scattering vector / reciprocal space vector, $\vec{q} = (q_x, q_y, q_z)^T$.
r_e	classical electron radius
	$r_e = e^2/4\pi\epsilon_0 mc^2 = 2.82 \times 10^{-5}$.
$\rho_e(\vec{r})$	electron density at position \vec{r} .
$\frac{d\sigma}{d\Omega}$	differential scattering cross section.
θ_f	azimuthal scattering angle (out-of-plane scattering angle).

1

Fundamentals

summarizes the content the aspects of ... relevant for
this investigation

This chapter covers the theoretical fundamentals of the interactions of x-rays with matter with a brief general overview. Since this thesis specifically covers the interaction of EUV and X-ray radiation with multilayer systems, the basic principles of specular reflection and transmission through a stack of layers are given. Then, the diffuse scattering theory for multilayer systems is derived based on the well established distorted-wave Born approximation (DWBA). Finally, the generation of fluorescence radiation and its exploitation for the analysis of multilayer compositions is described.

1.1 EUV and X-ray Radiation

EUV and X-ray denote specific spectral regions of the electromagnetic radiation.

Extreme ultraviolet (EUV) and x-ray radiation is electromagnetic radiation, which only differs by its spectral range. The different names for these parts of the electromagnetic spectrum are mostly of historic origin. However, differences in energy and, thus, reflectance, transmission and absorption properties in matter still justify this differentiation today from a technical perspective. For the sake of consistency within this thesis and the lack of a unique definition of the terms used in literature, we shall define EUV radiation as electromagnetic radiation within the spectral range from vacuum wavelength of 2 nm to 50 nm (corresponding to photon energies of approximately 620 eV to 25 eV). Consequently, the radiation with the vacuum wavelength from 0.01 nm to 2.0 nm (photon energies from around 124 keV to 0.62 keV) shall be called x-rays. In both cases the theoretical description is identical and is thus presented here independent of this naming convention.

The entirety of electrostatic fields and electromagnetic radiation is described by Maxwell's equations. In vacuum and without any electric charges present, they are defined as

$$\nabla \cdot \vec{E} = 0, \quad \nabla \cdot \vec{B} = 0,$$
$$\nabla \times \vec{E} = -\frac{\partial \vec{B}}{\partial t}, \quad \nabla \times \vec{B} = \mu_0 \epsilon_0 \frac{\partial \vec{E}}{\partial t},$$

+ the curl equations

$$\text{and using } \nabla \times (\nabla \times \vec{B}) = \nabla(\nabla \cdot \vec{B}) - \nabla^2 \vec{B}$$

with the electric constant ϵ_0 and the magnetic constant μ_0 and the electric field \vec{E} and the magnetic field \vec{B} . By taking the ~~curl~~^{curl} of the ~~two~~^{two} equations we obtain the wave equations for both fields as

$$\text{and } \frac{1}{c^2} = \mu_0 \epsilon_0 \quad \Delta \vec{E} - \frac{1}{c^2} \frac{\partial^2 \vec{E}}{\partial t^2} = 0, \quad \Delta \vec{B} - \frac{1}{c^2} \frac{\partial^2 \vec{B}}{\partial t^2} = 0, \quad (1.1)$$

where the speed of light in vacuum is defined as $c = 1/\sqrt{\mu_0 \epsilon_0}$. *it is!*

All scattering processes and charge densities in this thesis are considered to be time-independent. The wave equations Eq. (1.1) can thus be further simplified by separating the explicit time dependence of the fields as

$$\vec{E}(\vec{r}, t) = \vec{E}(\vec{r}) e^{i\omega t}, \quad \vec{B}(\vec{r}, t) = \vec{B}(\vec{r}) e^{i\omega t}, \quad (1.2)$$

where \vec{r} is a vector to a point in space. The time-independent wave equations then read

$$(\Delta + k_0^2) \vec{E} = 0, \quad (\Delta + k_0^2) \vec{B} = 0, \quad (1.3)$$

where $k_0 = \omega/c$, i.e. the modulus of the vacuum wave vector. A very important solution to this wave equation is the monochromatic plain wave, which is usually presumed to be impinging on scattering problems such as those discussed in this thesis. Hence, for Eq. (1.3) we obtain

explain: scattering problem

$$\vec{E}(\vec{r}, t) = E_0 e^{i\omega t - i\vec{k} \cdot \vec{r}}, \quad \vec{B}(\vec{r}, t) = B_0 e^{i\omega t - i\vec{k} \cdot \vec{r}}, \quad (1.4)$$

where E_0 and B_0 are the initial electric and magnetic field amplitudes, respectively, and $|\vec{k}| = k_0$ [7].

The radiation propagating as a plane wave has a wavelength of λ , where each photon carries an energy of

wave?

$$E_{ph} = \frac{hc}{\lambda} = \hbar\omega,$$

*also called de Broglie
wavenumber*

$$\omega = 2\pi f \quad (1.5)$$

where h is the Planck's constant and $\hbar = h/2\pi$. From this follows that the modulus of the vacuum wave vector, also called the *wave number*, $k_0 = 2\pi/\lambda$. The photon energy is typically expressed in units of the electron charge, which defines the unit *electron volt* (eV) used for expressions in this thesis.

This description of the propagation of electromagnetic radiation in vacuum can be extended to the propagation inside a homogeneous medium. This will be discussed in the following section on the interaction of EUV and x-ray radiation with matter.

1.2 Interaction of EUV and X-ray Radiation With Matter

As noted above, the wave equation Eq. (1.3) still holds for the propagation of radiation inside a homogeneous medium in slightly modified form. The speed of light c , while being a constant in vacuum with respect to the energy, becomes energy dependent once the wave enters the medium [2]. This dispersion has an impact on the wave number. In addition, in general the radiation will be partially absorbed while propagating through matter. To account for this change of the wave number with respect to the vacuum propagation we introduce a complex, energy dependent *index of refraction*,

$$n = 1 - \delta - i\beta, \quad (1.6)$$

*before go back to
Maxwell!*

$\mu_0 \rightarrow \mu$ $\epsilon_0 \rightarrow \epsilon$ in brackets, \rightarrow close!

where its real part δ accounts for the deviation from the vacuum index of refraction. The dispersion is a result of the interaction of the electromagnetic radiation with the electrons in the medium, which is dependent on the wavelength as well as the $\rho_e(\vec{r})$. The factor δ is therefore proportional to these two quantities $\delta \propto \lambda^2 \rho_e(\vec{r})$ [1, 25]. The absorption is accounted for by β , defined through the linear attenuation coefficient μ ,

$$\beta = \frac{\lambda \mu}{4\pi}. \quad (1.7)$$

explain!
and not
only!!
 \Rightarrow XAFS

By replacing the vacuum wave number k_0 with

$$k = nk_0 \quad (1.8)$$

in the wave equation Eq. (1.3) and the plain wave solutions in Eq. (1.4), we obtain the wave equation for the propagation of x-rays and EUV radiation inside a medium and its solutions.

\Rightarrow dielectric function, polarization, ...

Interaction of a Photon With Atoms and its Electrons

should be mentioned

} how?

The continuum description above gives a consistent description of the reflection, refraction and absorption of x-rays and EUV radiation at the interfaces of vacuum and matter in a macroscopic picture. The treatment is analogous to reflection and refraction in classical optics and serves well to describe these processes in case of specular reflectance from homogeneous materials as we shall see later in this chapter. However, it is necessary to also give a more general description on the interaction of a photon with the atoms, and more importantly the electrons, of a medium to describe the origin of the diffuse scattering and fluorescence processes, which are not covered by the continuum description above.

When a photon hits an atom with its electrons three very important process can occur, that need to be distinguished.

Elastic Scattering The photon interacts with the matter in an energy conserving way.

It may be scattered out of its original direction by interaction with single free electrons, also known as *Thomson scattering*. In general however, it might encounter ensembles of electrons, i.e. an electron density such as the bound electrons of an atom. This generalization of the scattering by an electron density is called *Rayleigh scattering*, which is highly photon energy dependent.

Rayleigh

\Rightarrow single scattering

\Rightarrow bound electrons

not in homogeneous media,

Inelastic Scattering In this case the photon exchanges a portion of its energy with the system it interacts with resulting in a loss of energy and, thus, increased wavelength for the scattered photon. This is the result of the particle-wave-duality of electromagnetic radiation. In this scattering process the total momentum of the incoming photon is conserved by scattering with an electron and transferring a portion of its momentum. This process is known as *Compton scattering*. In this picture the electron is treated as a free electron which ends up with an increased momentum. There is, however, the possibility that the photon excites a bound electron into an excited state thereby transferring its energy. This process is not covered by the Compton scattering process and is known as *Raman scattering*.

Absorption The third possibility is that the photon is absorbed entirely by ejecting a bound core shell electron from the atom leaving a vacancy. This is known as *photoelectric effect*. It requires a photon energy exceeding the binding energy of

What is
photo
electric
absorption?

Thomson \rightarrow Compton

is the same \rightarrow scatter of free electrons

fluorescence can also be optically excited → laser!

XRF

⇒ excitation

of core shells

⇒ electron into vacuum

instead of /

free (bonded) states

1.2.1 Elastic Scattering

Scattering of an incoming plane wave is described by the quantity of the differential scattering cross section, defined as

$$\left(\frac{d\sigma}{d\Omega}\right) = \frac{I_{\text{scattered}}}{\Phi_0 \Delta\Omega}, \quad I_s(\theta, \nu) = \Phi_0 \frac{d\Omega}{d\Omega} (1.9)$$

where $I_{\text{scattered}}$ is the scattered intensity into the solid angle $\Delta\Omega$ and Φ_0 is the total flux of incoming photons of the primary wave per unit area. Due to this proportionality, the goal of calculating the scattering intensity is achieved by determining the differential cross section for the scattering problem at hand. As an example we shall briefly demonstrate the differential cross section at hand of scattering from a single free electron and extend that description to scattering from an arbitrary electron density $\rho_e(\vec{r})$.

Rayleigh scattering from atoms

→ Rayleigh ⇒ Asymptotic

The scattering cross section in case of a single free electron is given by

$$\left(\frac{d\sigma}{d\Omega}\right) = \left(\frac{e^2}{4\pi\epsilon_0 mc^2}\right)^2 |\vec{e}_i \cdot \vec{e}_s|^2 = r_e^2 |\vec{e}_i \cdot \vec{e}_s|^2, \quad (1.10)$$

where e is the electron charge and the unit vectors \vec{e}_i and \vec{e}_s describe the direction of the electric field vector before and after the scattering process, respectively. The differential cross section in the case of *Thomson scattering* is proportional to the square of the classical electron radius r_e . Depending on the polarization properties of the impinging radiation, the scalar product of the two unit vectors yields

$$|\vec{e}_i \cdot \vec{e}_s|^2 = \begin{cases} 1 & \text{electric field perpendicular to scattering plane} \\ \cos^2(\Delta\Psi) & \text{electric field parallel to scattering plane} \\ \frac{1}{2}(1 + \cos^2(\Delta\Psi)) & \text{unpolarized radiation} \end{cases}, \quad (1.11)$$

where $\Delta\Psi$ is the angle between the incoming beam and the scatter direction (cf. Fig. 1.1 below) [1].

In general, the scattering from a single free electron will not be an accurate description for most scattering problems of radiation on matter. Instead electrons are bound in an atom and the radiation is scattered by the electron density at a certain position \vec{r} associated with the distribution of electrons in a certain atom. The result is a differential

cross section considering the scattering from a volume element $d\vec{r}$ by the electron density $\rho_e(\vec{r})$,

$$\left(\frac{d\sigma}{d\Omega} \right) = r_e^2 |f^0(\vec{q})|^2 |\vec{e}_i \cdot \vec{e}_s|^2 = r_e^2 \left| \int \rho_e(\vec{r}) e^{-i\vec{q} \cdot \vec{r}} d\vec{r} \right|^2 |\vec{e}_i \cdot \vec{e}_s|^2, \quad (1.12)$$

where $f^0(\vec{q})$ is called the *atomic form factor* and $\vec{q} = \vec{k}_f - \vec{k}_i$ the *wavevector transfer or scattering vector* [11]. The latter in Eq. (1.12) accounts for the phase difference between different scattering centers in the spacial electron distribution and is an important characteristic of any scattering process. Since the scattering processes described in this thesis are considered in reflection geometry only, we shall define it in terms of the corresponding incidence and exit angles below.

Momentum Transfer and Reciprocal Space

Assuming a scattering process from a single surface in reflection geometry as depicted in Fig. 1.1 the incoming beam irradiating the sample under the angle of incidence α_i is described by the wave vector \vec{k}_i . The direction of this vector is the propagation direction

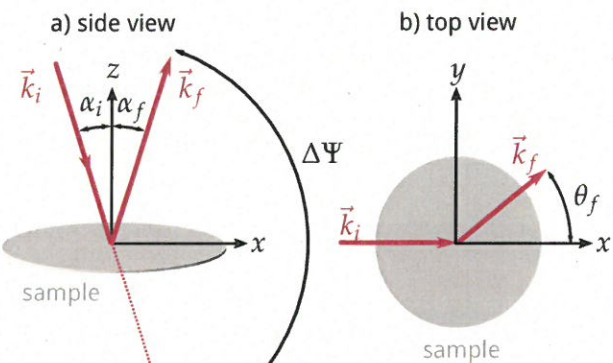


Figure 1.1 | Scattering geometry for the definition of the scattering vector \vec{q} .

wide die Kontaktlinien als rote und schwarze Punkte an

of the incident radiation, where its absolute value is the wavenumber $k = |\vec{k}_i| = \frac{2\pi}{\lambda}$. A detector positioned at a different angle, typically called scattering angle α_f , detects the scattered radiation. The outgoing or scattered beam is described by the wavevector \vec{k}_f with direction towards the detector, again in accordance with the propagation direction of the radiation. In case of an elastic, i.e. energy conserving, scattering process its absolute value is the wavenumber of the incoming beam $|\vec{k}_f| = |\vec{k}_i| = k_0$. This general scattering process is characterized by its momentum transfer vector

$$\vec{q} = \vec{k}_f - \vec{k}_i, \quad (1.13)$$

also known as scattering vector. From this definition the components of this three dimensional vector can be expressed by the involved angles and wavelengths as

$$\begin{aligned} q_x &= k(\cos \theta_f \sin \alpha_f - \sin \alpha_i), \\ q_y &= k(\sin \theta_f \sin \alpha_f), \\ q_z &= k(\cos \alpha_f + \cos \alpha_i). \end{aligned} \quad (1.14)$$

The momentum transfer vector is a characteristic quantity for scattering processes. Its three components in Eq. (1.14) span the so called reciprocal space.

Anomalous scattering and Born approximation

The differential cross section found in Eq. (1.12) with the atomic form factor $f^0(\vec{q})$ follows from a quantum mechanical perturbation calculation and is strictly speaking only valid far away from any electronic resonance. That, however, might not be the case, especially for EUV and x-ray radiation scattered on light elements. Here, especially the core shell energy levels are close to the energy of the impinging radiation. In that case the electron response will no longer be that of a free or quasi free electron but influenced due to the fact that it is tightly bound. This effect is called *dispersion* and results in two wavelength dependent dispersion correction factors in the atomic form factor [1, 11], which is described as

$$f(\vec{q}, \lambda) = f^0(\vec{q}) \cdot [f'(\lambda) + i f''(\lambda)] \quad f(\vec{q}, \lambda) = f^0(\vec{q}) + f'(\lambda) + i f''(\lambda). \quad (1.15)$$

The *atomic scattering factors* $f'(\lambda)$ and $f''(\lambda)$ are strongly dependent on the element of the atoms involved in the scattering process. The first factor $f'(\lambda)$ accounts for the modified response of an electron close to an electronic resonance, often described in analogy to a driven harmonic oscillator close to its eigenfrequency. The second factor $f''(\lambda)$ describes dissipative processes into the atomic system. It is associated with the absorption of radiation in matter. In fact, both factors, while being related through the so called *Kramers-Kronig relation*, define the complex index of refraction (expressed here for a single element) of the continuum theory introduced above at the beginning of Sec. 1.2 through

$$n = 1 - \delta - i\beta = 1 - \frac{r_e}{2\pi} \lambda^2 n_a f(0, \lambda), \quad (1.16)$$

where n_a is the number of atoms per unit volume [37].

Finally, we should note that the atomic form factor including its dispersion correction terms in Eq. (1.15) and consequently the differential scattering cross section from Eq. (1.12) is obtained following a perturbation theory approach. In the quantum mechanical description the field driving the scattering process is considered to be the incident wave field (e.g. a plane wave) instead of the exact total field including the scattered field component. This is an approximation, called the *Born approximation*, only valid if the scattered field is small compared to the incident field. This implicitly corresponds to considering only one single scattering event per incident photon. Multiple scattering processes are not included in this description (kinematic scattering). Later, we will generalize this approximation to more complex, exactly solvable scattering problems instead of considering only the kinematic processes.

1.2.2 Absorption and Fluorescence Radiation

Absorption of electromagnetic radiation, more specifically X-ray radiation, in matter is the third main interaction process mentioned here. In that case, the incoming photon is totally absorbed by a bound core shell electron and transfers all its energy to the electron leaving it in an energetically excited state. If the energy of the incoming is sufficient to excite the electron into the continuum above the binding energy, that electron is ejected from the atom leaving a vacancy at one of the core shells. Since this state is no longer the energetically most stable one, relaxation of electrons in energetically higher shells into the vacancy cause the release of energy. This can happen through two competing

Specular Reflectance from Surfaces and Interfaces in Multilayer Systems

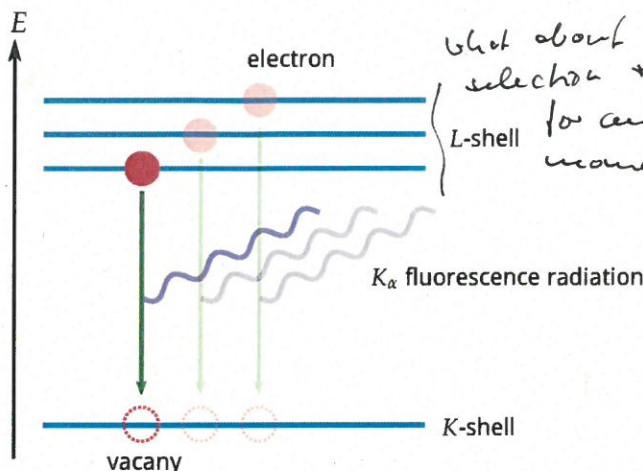


Figure 1.2 | Illustration of X-ray fluorescence for an atom. The relaxation of all possible L-shell electrons into the K-shell vacancy is shown. That leads to the emission of characteristic K_{α} fluorescence radiation at three different energies. The figure is not to scale.

processes known as *X-ray fluorescence* and the *Auger effect*. The general principle of X-ray fluorescence is illustrated in Fig. 1.2.

Each material exhibits a sharp increase in the interaction cross section when irradiated with increasing photon energy. Those jumps correspond to the K, L and M absorption edges of the core shell electrons leading to photoionization of that particular atom creating the above mentioned vacancy. Since the electronic structure of the core shell is specific to a particular element, the emitted fluorescence radiation is characteristic for the material in the sample. That fact is exploited in the X-ray fluorescence (XRF) analysis, where the amount of a specific chemical element inside of matter can be determined by measuring the spectral distribution of the fluorescence radiation.

Instead of emitting fluorescence radiation the energy of the relaxation process into the vacancy can be transferred radiation less to a secondary electron with lower binding energy than the primary, excited electron. In that case, given sufficient energy, the secondary electron can also be ejected with a overall reduced kinetic energy compared to the primary electron. This is the Auger process. Since, again, the binding energy of the secondary electron is specific for the chemical element, **Auger electron spectroscopy** also yields information on the material composition. The two processes of fluorescence and Auger emission compete. For elements with low atomic number Z , the Auger process dominates while almost no fluorescence is present. With increasing atomic number the ratio reverses resulting in a higher fluorescence yield than Auger electron yield for high Z elements.

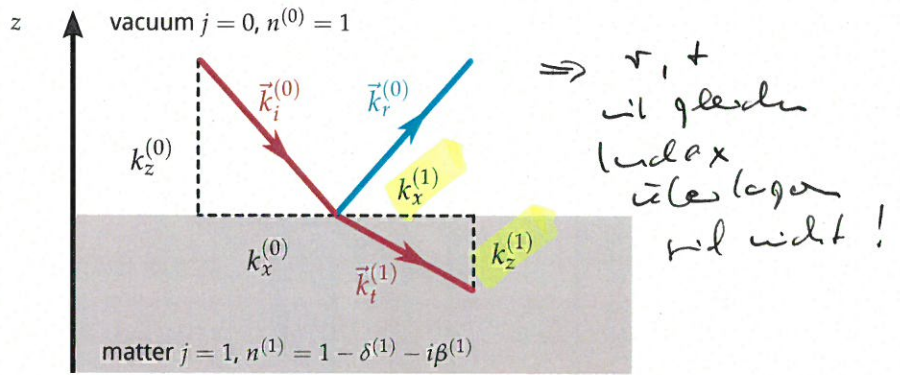
rob
Fader

1.3 Specular Reflectance from Surfaces and Interfaces in Multilayer Systems

As mentioned above in the beginning of Sec. 1.2 the reflection and transmission of EUV and x-ray radiation will be treated here with a continuum approach based on the index of refraction. Before we treat specular reflectance and transmittance in multilayer systems, lets recapitulate reflection and transmission through a single surface. Fig. 1.3 gives the necessary definitions for radiation passing through an abrupt interface. The coordinate system was chosen such that the surface is perpendicular to the z -direction and $z = 0$ is at the surface. The refraction process in that case is entirely governed by *Snell's law*

FUNDAMENTALS

Figure 1.3 | Illustration of Snell's law. The parallel component of the wave vector $k_x^{(0)} = k_x^{(1)} = k_x$ remains unchanged when the radiation enters the medium. The perpendicular component changes according to the index of refraction (see main text).



known from classical optics [7]. With the solutions of the wave equation for propagation in homogeneous media in the beginning of Sec. 1.2, Snell's law can be expressed in terms of the wave vector by

$$k_z^{(j)} = \sqrt{(n^{(j)}k_0)^2 - k_x^2} \quad , \text{ with } k_x = \cos(\alpha_i)k_0, \quad (1.17)$$

and the angle of incidence α_i defined from the surface normal (cf. Fig. 1.1) and $n^{(j)}$ is the complex index of refraction of layer j .

Another well known requirement at the interface is the continuity of both the electric field amplitude and its derivative [7, 15]. From that follows that the parallel component of the wave vector $k_x^{(j)} \equiv k_x \forall j$ does not change at the interface. Together with the relation in Eq. 1.8 this yields a relation of the electric field amplitudes in vacuum (layer $j = 0$) and the medium (layer $j = 1$) through the Fresnel coefficients of reflection $r^{(0)}$ and transmission $t^{(0)}$ via

liegt schon Index

$$\left(\begin{array}{c} E_t \\ E_r \end{array} \right) = \left(\begin{array}{c} t^{(0)} E_0 \\ r^{(0)} E_0 \end{array} \right), \quad (1.18)$$

where E_0 is the field amplitude of the incident field with wave vector $\vec{k}_i^{(0)}$, $E_t^{(1)}$ is the transmitted field amplitude in layer $j = 1$ with wave vector $\vec{k}^{(1)}$ and $E_r^{(0)}$ is the reflected field amplitude with wave vector $\vec{k}_r^{(0)}$. For the transmission and reflection at any two interfaces j and $j + 1$ the Fresnel coefficients read

$$r^{(j)} = \frac{k_z^{(j)} - k_z^{(j+1)}}{k_z^{(j)} + k_z^{(j+1)}}, \quad (1.19)$$

$$t^{(j)} = \frac{2k_z^{(j)}}{k_z^{(j)} + k_z^{(j+1)}}. \quad (1.20)$$

Matrix Algorithm for Multilayer Systems

In this part we extend the calculation above to a system of multiple layers on top of a substrate which is assumed to be infinite. This provides the exact fully dynamic solution of the wave equation for an ideal multilayer system with abrupt interfaces. Thus, all reflections and transmissions at all interfaces are considered, including multiple events. The EUV and X-ray fields were calculated based on the well-established matrix algorithm which is an extension of the above Fresnel coefficient method [7, 25]. The field inside each layer j is described similarly to Eq. (1.18) by their reflected and transmitted field components as

$\Rightarrow \text{S. Fig. 1.3}$

$$E^{(j)}(\vec{r}) = e^{i\vec{k}_{\parallel} \cdot \vec{r}_{\parallel}} (E_t^{(j)}(z) + E_r^{(j)}(z)), \quad (1.21)$$

where \vec{k}_{\parallel} is the wave vector component parallel to the interfaces (in the two-dimensional geometry of Fig. 1.3 above was $\vec{k}_{\parallel} = \vec{k}_x$) and \vec{r}_{\parallel} is the position perpendicular to the z -direction. The two field components are further described by the transmitted and reflected field amplitudes T_j and R_j as

$$E_t^{(j)}(z) = T_j e^{ik_z^{(j)} z}, \quad (1.22)$$

$$E_r^{(j)}(z) = R_j e^{-ik_z^{(j)} z}, \quad (1.23)$$

where $E_t^{(j)}(z)$ describes the field component propagating towards the substrate and $E_r^{(j)}(z)$ is the reflected field component in each layer propagating towards the vacuum. The field amplitudes and layer thicknesses are illustrated in Fig. 1.4. The components of

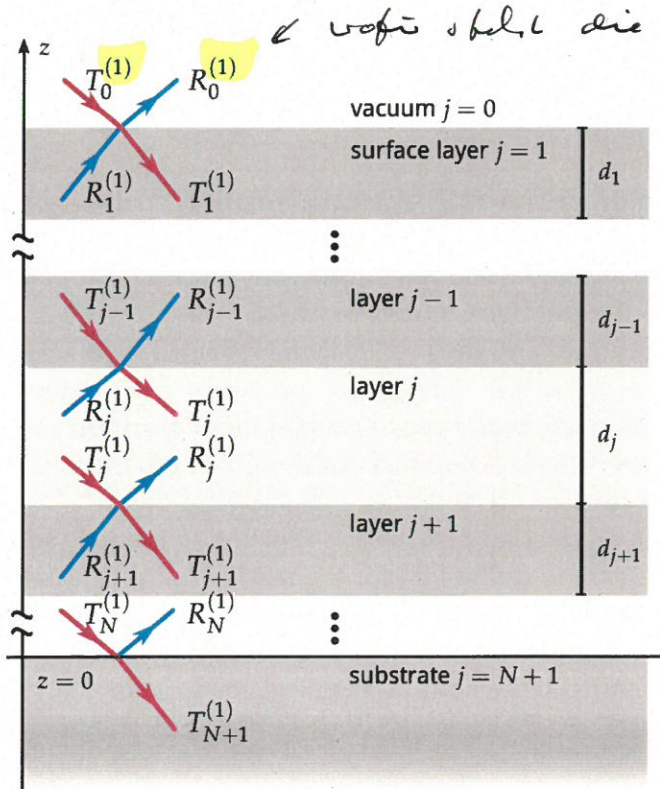


Figure 1.4 | Illustration of the field amplitudes in the exact analytical solution of field propagation through a multilayer stack. The vertical coordinate z is defined to be zero at the substrate interface. The field amplitude of the incident field in the vacuum T_0 is known. Inside the infinite substrate no reflected field amplitude exists, i.e. $R_{N+1} = 0$. The layer thicknesses are denoted d_j for the j th layer.

FUNDAMENTALS

two adjacent layers are connected by the propagation matrix M_j

$$M_j = \frac{1}{t^{(j)}} \begin{pmatrix} 1 & r^{(j)} \\ r^{(j)} & 1 \end{pmatrix} \begin{pmatrix} e^{-ik_z^{(j+1)}d_{j+1}} & 1 \\ 1 & e^{ik_z^{(j+1)}d_{j+1}} \end{pmatrix}, \quad (1.24)$$

through the relation

$$\begin{pmatrix} E_t^{(j)} \\ E_r^{(j)} \end{pmatrix} = M_j \begin{pmatrix} E_t^{(j+1)} \\ E_r^{(j+1)} \end{pmatrix}. \quad (1.25)$$

The field propagation matrix in Eq. (1.24) includes the Fresnel coefficients from Eq. (1.19) and Eq. (1.20) accounting for the reflection and transmission process at the interface. In between two interfaces a homogeneous layer was assumed so that the field is only propagated by the phase factor $e^{\pm ik_z^{(j)} d_j}$ along the z -direction and the layer thickness d_j . The system of equations in Eq. (1.25) becomes solvable by replicated application of the field propagation matrix to relate the *known* incident field amplitude E_0 , the total reflected field amplitude in the vacuum E_R and the transmitted field in the substrate E_T . Since there can not be a reflected field inside the substrate the system of equations Eq. (1.25) reads

$$\begin{pmatrix} E_0 \\ E_R \end{pmatrix} = \prod_j M_j \begin{pmatrix} E_T \\ 0 \end{pmatrix}, \quad (1.26)$$

with two unknowns E_R and E_T which can be calculated based on this relation. Thereby all field amplitudes at each interface can be obtained. The total reflectance R and transmittance T can then be calculated as the quotient of the (known) incoming field E_0 with the reflected E_R and transmitted field E_T , respectively, as

$$\begin{aligned} R &= |E_R/E_0|^2, \\ T &= |E_T/E_0|^2. \end{aligned} \quad (1.27)$$

Accounting for Roughness and Interdiffusion

*exact known case
and topography*

The calculation above yields an exact and fully dynamic solution of the problem of reflecting and transmitting EUV or x-ray radiation from and through a generic multilayer. However, in a realistic sample the interfaces will not be perfectly flat and abrupt. Instead the two materials could mix or the interfaces could be rough. Both effects lead to a diminished reflectance of each interface and thus reduce the reflected field amplitudes which changes their interference behavior. These two processes of roughness and interdiffusion can be treated within the framework of the matrix algorithm presented above by using modified Fresnel coefficients. A detailed calculation for arbitrary roughness profiles along the z -direction can be found in [38], for example.

For our calculations we assume a Gaussian distribution function of the roughness and interdiffusion. The general expression found in [38] for the modified Fresnel coefficients then yields the result of Nérot and Croce [9, 26]. The Gaussian distribution function corresponds to the assumption of the interdiffusion and roughness profile to be of error-function like shape, which leads to the modified Fresnel coefficients

$$\begin{aligned} \tilde{r}^{(j)} &= r^{(j)} \exp(-2k_z^{(j)} k_z^{(j+1)} \sigma_j^2), \\ \tilde{t}^{(j)} &= t^{(j)} \exp((k_z^{(j)} - k_z^{(j+1)})^2 \sigma_j^2 / 2), \end{aligned} \quad (1.28)$$

where $r^{(j)}$ and $t^{(j)}$ are the unmodified Fresnel coefficients for an ideal multilayer system at each interface j from Eq. (1.19) and Eq. (1.20). The parameter σ_j is the *mean square roughness* or *interdiffusion*, respectively at the j th interface. For any calculation within the framework of this thesis, those modified Fresnel coefficients were used in Eq. (1.24) instead of the ideal coefficients.

1.4 Diffuse Scattering in Layered Systems

Diffuse scattering in the special case of layered systems is the result of imperfections of surfaces or interfaces, which otherwise show only specular (coherent) reflectance. In Sec. 1.2.1 we have elaborated the elastic scattering of EUV and X-ray radiation on single electrons and atoms. The underlying assumption, also known as Born approximation, is that the scattering is weak with respect to the incoming primary wave. The scattering process thus only considers the primary wave, typically a plane wave, and not the total wave field including the scattered radiation in the theoretical description of the process. This is equivalent to the assumption of a single scattering event ignoring multiple scattering, also known as kinematic scattering. In the context of layered systems, diffuse scattering is described within the framework of perturbation theory. (DWBA)

In this case, in terms of the conventional Born approximation that corresponds to treating the existence of and potential disturbances within a multilayer system as perturbation. The approximation would then consider the scattered radiation to be weak with respect to the impinging plane wave. The latter is then simply the exact solution to the vacuum wave equation Eq. (1.3). This approximation, however, is most certainly not valid in case of the presence of a multilayer system which significantly alters the incoming plane wave in the reflection and transmission process.

Instead, theoretical description of the diffuse EUV scattering from multilayers is based on the DWBA [21, 22], widely used in the analysis of hard X-ray scattering. The DWBA is an extension of the above mentioned Born approximation in which the interfacial roughness is considered to be a small deviation from the ideal multilayer system. In general, the wave equation for a multilayer system is

$$(\Delta + k_0^2)E(\vec{r}) = V(\vec{r})E(\vec{r}), \quad (1.29)$$

with the potential $V(\vec{r}) = k_0(1 - n^2(\vec{r}))$ [27] describing the different materials inside the layer system through their index of refraction n . The DWBA is based on the principle that part of this potential leads to a wave equation which can be solved analytically, while a small disturbance to that potential remains to be treated as perturbation. In case of a multilayer the exact solution of a system with ideal interfaces can indeed be found and is given in Sec. 1.3. The potential can be separated into a strong part $V_{\text{id}}(\vec{r})$ for which an analytical solution exists and a small perturbation $V_r(\vec{r})$ describing the interfacial roughness as deviation from the ideal layer system, i.e. $V(\vec{r}) = V_{\text{id}}(\vec{r}) + V_r(\vec{r})$. In analogy to the Born approximation, the scattering process is then evaluated considering the wave fields obtained from the solution with the ideal potential $V_{\text{id}}(\vec{r})$ only. Instead of the full wave field including all previous scattering events. Thus, the analytic solution of the multilayer wave equation ("distorted wave") in the DWBA takes the place of the plane wave in the Born approximation. In that way, the scattering from the perturbations are still considered kinematically (single scattering approximation), however, the incoming distorted waves are fully dynamic solutions of the transmittance and reflectance at all layers of the multilayer system.

and then calculating a first iteration with the full potential

$$\rightarrow (\Delta + k_0^2)E(\vec{r}) = (V_{\text{id}} + V_r)E(\vec{r}) \quad (\text{and } \dots ?)$$

eine Reihe dieser Art sollte hier stehen

1.4.1 The DWBA Scattering Cross Section

The detailed derivation of the diffuse (incoherent) differential scattering cross section for rough multilayer systems can be found in Pietsch, Holý and Baumbach [27] and the corresponding publications [21, 33], as well as in de Boer [6] and Mikulík [25]. Here, we give a summarized version illustrating the application to near-normal incidence scattering and the corresponding approximations leading to the determination of a roughness power spectral density (PSD) for the interfaces in a multilayer system.

The derivation of the diffuse scattering cross section is based on the quantum mechanical formalism for perturbation theory. There, the transition probability from one state into another is described as the expectance value of the transition matrix. In case of the scattering problem at a multilayer this translates to considering the incoming wave field, given by the exact solution of the wave equation for a multilayer system and calculating the expectance value for scattering into a scattered state arriving at the detector. The latter is generally unknown. However, the reciprocity theorem [23, 24] of classical electrodynamics states that an unknown field at a detector generated by a known dipole source, i.e. the incident field induced dipole at a perturbation of an interface causing the emission of scattered radiation, can be replaced by the time-inverted known field caused by a single dipole source at the detector position ("detector beam") [10, 21, 33]. The latter is just the time-inverted solution of the same wave equation of the ideal multilayer as for the regular solution. We thus consider two independent solutions of the wave equation (1.29) with $V(\vec{r}) = V_{\text{id}}(\vec{r})$ and express them in Dirac notation [13] as $|E_{\text{id}}^{(1)}\rangle$ and $|E_{\text{id}}^{(2)}\rangle$, where the superscript (1) denotes the regular solution obtained via the matrix algorithm in Sec. 1.3 and the index (2) indicates the time-inverted solution for the scattering angle α_f of the detector position with respect to the surface.* According to Eq. (1.21), Eq. (1.22) and Eq. (1.23) the two solutions can be expressed in terms of the reflected and transmitted field amplitudes as

$$|E_{\text{id}}^{(1)}\rangle = e^{i\vec{k}_{\parallel,(1)} \cdot \vec{r}_{\parallel}} (T_j^{(1)} e^{ik_z^{(j)} z} + R_j^{(1)} e^{-ik_z^{(j)} z}), \quad (1.30)$$

$$|E_{\text{id}}^{(2)}\rangle = (\langle E_{\text{id}}^{(2)} |)^* = e^{-i\vec{k}_{\parallel,(2)} \cdot \vec{r}_{\parallel}} (T_j^{(2)*} e^{-ik_z^{(j)} z} + R_j^{(2)*} e^{ik_z^{(j)} z}). \quad (1.31)$$

These solutions are the basis for the calculation of the differential scattering cross section, which is given by the covariance of the matrix element of the perturbation potential [27] as

$$\left(\frac{d\sigma}{d\Omega} \right)_{\text{DWBA}} = \text{Cov}(\langle E_{\text{id}}^{(2)} | V_r | E_{\text{id}}^{(1)} \rangle). \quad (1.32)$$

The explicit expression for the covariance can be calculated based on Eq. (1.30) and Eq. (1.31) and yields the full DWBA differential scattering cross section for the diffuse (incoherent) scattering considering all transmitted and reflected fields, i.e. all first order dynamic effects, as

$$\begin{aligned} \left(\frac{d\sigma}{d\Omega} \right)_{\text{DWBA}} = & \left[\frac{A\pi^2}{\lambda^4} \sum_{j=1}^N \sum_{i=1}^N (n_j^2 - n_{j+1}^2)^* (n_i^2 - n_{i+1}^2) \right. \\ & \times (T_i^{(1)} + R_i^{(1)}) (T_i^{(2)} + R_i^{(2)}) \Big] S_{ij}(\vec{q}_{\parallel}; q_z^{(j)}, q_z^{(i)}), \end{aligned} \quad (1.33)$$

* In regard to the matrix algorithm in Sec. 1.3 the solution for the time-inverted "detector beam" is obtained by replacing the vacuum wave vector component k_x in Eq. (1.17) with the corresponding component for the scattering angle α_f instead of the angle of incidence α_i .

where A is the illuminated sample area and $S_{ij}(\vec{q}_{\parallel}; q_z^{(j)}, q_z^{(i)})$ includes the effect of the perturbation potential $V_r(\vec{r})$. For the multilayer system this perturbation is roughness at the interfaces, which can be correlated vertically throughout the stack, as well as in-plane of a single interface. A detailed derivation of the explicit form of that form factor is given in the following paragraph.

In the case of small reflectivity amplitudes, dynamic multiple reflections are often neglected and the dominant term in the decomposition is diffuse scattering of the transmitted fields at the roughness of each interface. The so-called semi-kinematic approximation [33] yields an explicit expression for Eq. (1.32) with

$$\begin{aligned} \text{semi-kinematic} \\ \left(\frac{d\sigma}{d\Omega} \right)_{\text{DWBA}} &= \frac{A\pi^2}{\lambda^4} \sum_{j=1}^N \sum_{i=1}^N ((n_j^2 - n_{j+1}^2)^* (n_i^2 - n_{i+1}^2) \\ &\times T_j^{(1)*} T_j^{(2)*} T_i^{(1)} T_i^{(2)} S_{ij}(\vec{q}_{\parallel}; q_z^{(j)}, q_z^{(i)})). \end{aligned} \quad (1.34)$$

The semi-kinematic approximation is similar to the conventional Born approximation, except that it considers the exact transmitted field amplitudes at a certain interface instead of a plane wave. The comparison of this expression with the full first-order DWBA term in Eq. (1.33) is useful to evaluate the contribution of dynamic effects to the scattering cross section and consequently the measured diffuse scattering distribution.

An illustration of the four scattering processes included in the full first-order DWBA is shown in Fig. 1.5 at the example of the interface of layer j and $j + 1$ in the multilayer system.

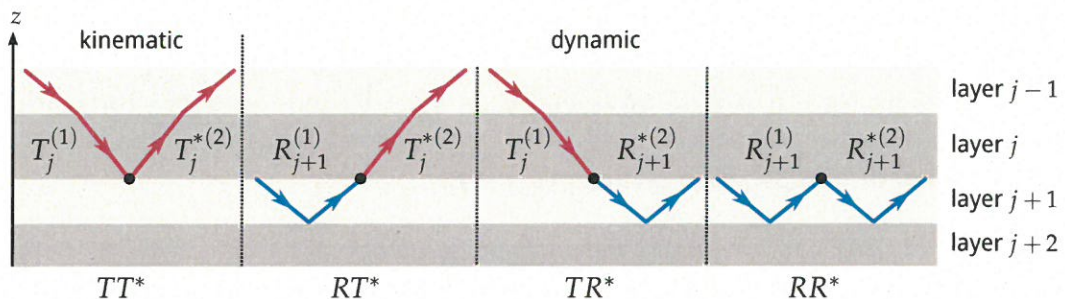


Figure 1.5 | Illustration of the four scattering processes of the DWBA^a. The TT^* process on the left is purely kinematic in nature and equivalent to the Born approximation. The three other processes RT^* , TR^* and RR^* are purely dynamic and not described by kinematic theory.

^a Figure similar to Pietsch, Holý and Baumbach [27].

Calculation of the Roughness Power Spectral Density

The effect of the perturbation potential is contained within the factor $S_{ij}(\vec{q}_{\parallel}; q_z^{(j)}, q_z^{(i)})$ in Eq. (1.33) and Eq. (1.34). For a multilayer system this perturbation is interfacial roughness as a deviation from the ideal multilayer with sharp and perfectly flat interfaces. The influence of the interfacial roughness on the diffuse scattering intensity described by the

FUNDAMENTALS

explicit form [5, 6]

$$S_{ij}(\vec{q}_\parallel; q_z^{(j)}, q_z^{(i)}) = \frac{\exp \left[-((q_z^{(j)*})^2 \sigma_j^2 + (q_z^{(i)})^2 \sigma_i^2)/2 \right]}{q_z^{(j)*} q_z^{(i)}} \times \int d^2 \vec{X} \left(\exp[q_z^{(j)*} q_z^{(i)} C_{ij}(\vec{X})] - 1 \right) \exp(i \vec{q}_\parallel \cdot \vec{X}), \quad (1.35)$$

where $q_z^{(i)}$ is the z-component of the scattering vector \vec{q} at the i th interface, $\vec{X} = \vec{x} - \vec{x}'$ is the lateral distance vector and $C_{ij}(\vec{x} - \vec{x}') = \langle h_i(\vec{x}) h_j(\vec{x}') \rangle$ is the height correlation function of the interface profiles $h(\vec{x})$ of the interfaces i and j , respectively. The factor σ_j is the root mean square (r.m.s.) roughness of the j th interface.

We consider the situation, where the roughness is small in relation to the scattering vector. This assumption is valid especially for high-quality multilayer systems as the mirrors considered in the framework of this thesis. This is the so-called small roughness approximation. In that case, the product of roughness and the z-component of the scattering vector is small, i.e. $q_z^{(j)} \sigma_j \ll 1$. We therefore can approximate the first part of Eq. (1.35) by

$$\frac{\exp \left[-((q_z^{(j)*})^2 \sigma_j^2 + (q_z^{(i)})^2 \sigma_i^2)/2 \right]}{q_z^{(j)*} q_z^{(i)}} \approx \frac{1}{q_z^{(j)*} q_z^{(i)}} \quad (1.36)$$

and Taylor expand the integrand as $\exp[q_z^{(j)*} q_z^{(i)} C_{ij}(\vec{X})] - 1 \approx q_z^{(j)*} q_z^{(i)} C_{ij}(\vec{X})$. With these approximations Eq. (1.35) reduces to

$$S_{ij}(\vec{q}_\parallel) \approx \int d^2 \vec{X} C_{ij}(\vec{X}) \exp(i \vec{q}_\parallel \cdot \vec{X}). \quad (1.37)$$

$S_{ij}(\vec{q}_\parallel)$ is, thus, the Fourier transform of the correlation function $C_{ij}(\vec{X})$. Assuming identical growth for the individual layers, i.e. a material independent propagation of roughness along the z-direction, $S_{ij}(\vec{q}_\parallel)$ can be expressed in terms of the lateral PSD $C_i(\vec{q}_\parallel)$ and a vertical replication factor $c_{ij}^\perp(\vec{q}_\parallel)$ [35],

$$S_{ij}(\vec{q}_\parallel) = c_{ij}^\perp(\vec{q}_\parallel) C_{\max(i,j)}(\vec{q}_\parallel). \quad (1.38)$$

Other PSD functions based on different models of lateral interface roughness correlation have been proposed, e.g. by Sinha et al. [33]. We follow the approach by de Boehr et al. [3, 5] for fractal interface roughness, where the lateral correlation function of the i th interface is given by

$$\tilde{C}_i(\vec{X}) = P_i \xi_\parallel^{H_i} |\vec{X}|^{H_i} K_{H_i}(|\vec{X}|/\xi_\parallel). \quad (1.39)$$

H_i is the Hurst factor providing a measure for the jaggedness of the interface [33], K_{H_i} are the modified Bessel functions of the order H_i , ξ_\parallel is a lateral correlation length and

$$P_i = \frac{\sigma_i^2}{\xi_\parallel^{H_i-1} 2^{H_i-1} \Gamma(1+H_i)/H_i}. \quad (1.40)$$

Our goal is to determine a single average power spectral density. We thus do not distinguish between individual interfaces in the model and assume identical roughness

properties for all interfaces. Hence $\sigma_j = \sigma$, $H_j = H$ and $C_{\max(i,j)}(\vec{q}_\parallel) = C(\vec{q}_\parallel)$. The PSD is given by the Fourier transform of Eq. (1.39) with respect to q_x , which yields the closed analytic form

$$C(\vec{q}_\parallel) = \frac{4\pi H\sigma^2 \xi_\parallel^2}{(1 + |\vec{q}_\parallel|^2 \xi_\parallel^2)^{1+H}}. \quad (1.41)$$

Vertical correlation of roughness

The high degree of thickness stability for well-defined multilayers as is necessary for high-performance mirrors implies a high degree of vertical correlation of individual interfaces roughness throughout the stack. In order to derive the replication factor in Eq. (1.38), we follow Stearns et al. [36]. In this model, the evolution of the surface roughness $w(x, y)$ during the growth of a single layer is described by the Langevin equation. In its Fourier transformed form,

$$\frac{\partial w(f)}{\partial t} = -4\pi^2 v f^2 w(f) + \frac{\partial \eta(f)}{\partial t}, \quad (1.42)$$

where v is a diffusion-like parameter, $\eta(f)$ is random noise normalized to the layer thickness and $w(f)$ describes the roughness evolution in dependence of the spatial frequency f . The roughness evolution during the growth of a single layer of a specific material can then be evaluated by discretizing Eq. (1.42) for the successive deposition of material of thickness δd

$$w_i(f) = c_\perp(f; \delta d) w_{i-1}(f) + \eta(f), \quad (1.43)$$

where $c_\perp(f; \delta d)$ is the replication factor of roughness for a single deposition. In the limit of repeated infinitesimal depositions until the full n th layer of thickness d_n is grown, $c_\perp(f, d_n)$ can be evaluated to be [35]

$$\begin{aligned} c_\perp(f, d_n) &= \exp(-4\pi^2 f^2 v d_n) \\ &= \exp(-|\vec{q}_\parallel|^2 v d_n), \end{aligned} \quad (1.44)$$

with $|\vec{q}_\parallel|^2 = 4\pi^2 f^2$. Assuming identical diffusion-like behavior v for all materials of a multilayer and defining $\xi_\perp(\vec{q}_\parallel) = 1/(v|\vec{q}_\parallel|^2)$, the replication factor in Eq. (1.38) is given by

$$c_{ij}^\perp(\vec{q}_\parallel) = \exp\left(-\sum_{n=\min(i,j)}^{\max(i,j)-1} d_n / \xi_\perp(\vec{q}_\parallel)\right). \quad (1.45)$$

Here, $\xi_\perp(\vec{q}_\parallel)$ can be interpreted as a spatial frequency dependent vertical correlation length, describing the distance perpendicular to the stack until the replication factor decreased to $1/e$.

and eigefeld!

Off-Axis Vertical Roughness Correlation

Gullikson et al. [16] observed that the direction of the vertical replication of roughness can be tilted with respect to the surface normal. This leads to tilted Bragg planes requiring a coordinate transformation in reciprocal space to account for the tilt angle β according to

$$\bar{q}_z = q_z - \hat{e} \cdot \vec{q}_{\parallel} \tan \beta, \quad (1.46)$$

where \hat{e} is a unit vector in direction of the roughness replication. Since the vertical scattering vector components enter the calculations through the Fresnel coefficients in Eq. (1.19) and Eq. (1.20), an additional factor appears in the calculation of Eq. (1.38) through substitution by

$$\overline{S_{ij}}(q_x) = \exp \left(-i\hat{e} \cdot \vec{q}_{\parallel} \tan \beta (z_i - z_j) \right) S_{ij}(q_x), \quad (1.47)$$

where z_i is the z -position of the i th interface.

Full DWBA expression for near-normal incidence scattering

Taking together all the above findings and inserting them into Eq. (1.33), the full explicit expression for the DWBA scattering cross section on high-quality multilayer systems is given by

$$\begin{aligned} \left(\frac{d\sigma}{d\Omega} \right)_{\text{DWBA}} = & \left[\frac{A\pi^2}{\lambda^4} \sum_{j=1}^N \sum_{i=1}^N (n_j^2 - n_{j+1}^2)^* (n_i^2 - n_{i+1}^2) \left((T_j^{(1)} + R_j^{(1)})^* (T_j^{(2)} + R_j^{(2)})^* \right. \right. \\ & \times (T_i^{(1)} + R_i^{(1)}) (T_i^{(2)} + R_i^{(2)}) \Big) \exp \left(-iq_x \tan \beta (z_i - z_j) \right) c_{\perp}^{ij} \Big] C(q_x). \quad (1.48) \end{aligned}$$

Since all experiments in this thesis have been conducted in co-planar geometry, i.e. for in-plane scattering measurements with a vanishing azimuthal angle θ_f in Fig. 1.1, the parallel component of the scattering vector \vec{q} is given by its q_x component only, i.e. $\vec{q}_{\parallel} \equiv q_x$, by choice of the coordinate system for the reciprocal space. We define the x , y and z components of the reciprocal space vector in Eq. (1.14) to be parallel to the respectively labeled real space vectors in Fig. 1.1. The angle β is thus determined based on that scattering direction only and dependent on the direction from which the sample is irradiated. The replication factor c_{\perp}^{ij} and the PSD then read

$$c_{\perp}^{ij}(q_x) = \exp \left(- \sum_{n=\min(i,j)}^{\max(i,j)-1} \frac{d_n q_x^2}{\xi_{\perp}} \right), \quad (1.49)$$

where the definition $\xi_{\perp} = 1/v$ holds and

$$C(q_x) = \frac{4\pi H \sigma^2 \xi_{\parallel}^2}{(1 + q_x^2 \xi_{\parallel}^2)^{1+H}}, \quad (1.50)$$

in the explicit expression of Eq. (1.48).

In addition it should be noted here, that Eq. (1.48) separates the contribution to the scattering distribution of the multilayer and vertical correlation (in square brackets) on the one hand and the in-planar roughness represented through the PSD $C(q_x)$ on the other hand.

1.5 Grazing-incidence X-ray Fluorescence

Grazing-incidence X-ray fluorescence analysis is an established method to characterize the chemical composition of materials through the irradiation of samples with x-rays. It is based on the emission of characteristic fluorescence radiation, as elaborated on in Sec. 1.2.2. By irradiating an unknown sample with photons of sufficiently high energy, those photons are absorbed leaving the characteristic vacancies in the K, L and M core shells. The emission of isotropic fluorescence radiation then follows through recombination processes detected outside the sample. A quantitative analysis was developed by Sherman [31] and refined by others [8, 29, 32]. The *Sherman equation* links the emitted and measured characteristic fluorescence radiation to the material concentration of a specific chemical species via fundamental parameters and the measurement characteristics (experimental parameters) [30]. The quantitative analysis requires a detailed knowledge of the fundamental parameters as well as all experimental parameters. It is thus a very elaborate procedure. However, for periodic multilayer structures, a relative analysis of the measured fluorescence yield already delivers valuable spatial information on the distribution of chemical species.

Here, we therefore focus on the treatment of fluorescence emission by periodic multilayer systems, which posses a Bragg resonance, i.e. a pair of angle of incidence and photon energy which cause constructive interference at the interfaces. Before entering the details, let us review the aspects of generation of fluorescence radiation. The appearance of fluorescence radiation is linked with the electromagnetic field intensity of the impinging radiation for each infinitesimal volume element inside the sample through a proportionality

$$\rightarrow \text{absorption only where the photons go}$$

$$I_{\text{SXF}} = C \int |E(\vec{r})|^2 \rho(\vec{r}) d^3r, \quad (1.51)$$

where C is a constant, $|E(\vec{r})|^2$ is the field intensity and, here, $\rho(z)$ is the relative density at the position \vec{r} of the chemical species of which the characteristic fluorescence radiation intensity is measured. This expression is an approximation, since it ignores any self-absorption effects that may occur during the propagation of the fluorescence radiation through the material before reaching the detector. However, for strongly periodic systems as we shall discuss in this chapter, and a relative comparison of the intensities the effect of self-absorption becomes negligible. \rightarrow nicht verbreitert, aber es ist eine endliche und endliche Breite.

In case of laterally infinitely extended and invariant multilayer systems, i.e. for samples which are larger than any impinging beam and have the same layer stacking for all these points, the field intensity $|E(\vec{r})|^2$ only varies with the vertical coordinate z and thus reduces to $|E(\vec{r})|^2 = |E(z)|^2$ for a given angle of incidence and photon energy [4]. If the layer stacking is known, that intensity can be calculated with the matrix formalism elaborated on in Sec. 1.3. The intensity of the fluorescence radiation from those systems simplifies Eq. (1.51) to

$$I_{\text{SXF}} = \tilde{C} \int_0^D |E(z)|^2 \rho(z) dz, \quad (1.52)$$

where D is the total thickness of all layers of the stack and $E(z) = E_t^{(i)}(z) + E_r^{(i)}(z)$ is given by Eq. (1.22) and Eq. (1.23) for the respective layer i depending on the coordinate z. We define d_i as the thickness of each layer i , and thus $D = \sum_i d_i$. This formula is only

FUNDAMENTALS

valid if the fluorescence radiation is not emitted by the substrate on which the multilayer stack was deposited, since in that case the wave intensity inside the substrate has to be considered as well.

The integral in Eq. (1.52) has to be evaluated for all points z inside each layer i . The matrix algorithm as outlined in Sec. 1.3 yields only the field amplitudes at the interfaces of two materials of the stack. To numerically evaluate the integral we thus discretize the multilayer stack by subdividing the whole stack and thereby each layer into equidistant sublayers with a sufficient number of samples*. Fig. 1.6(a) shows an exemplary Cr/Sc multilayer system with the relative Sc density ρ_{Sc} in each layer. In order to numerically calculate the integral in Eq. (1.52), the system was divided into sublayers of thickness d_i and bottom interface positions z_i as described above and illustrated in Fig. 1.6(b). The

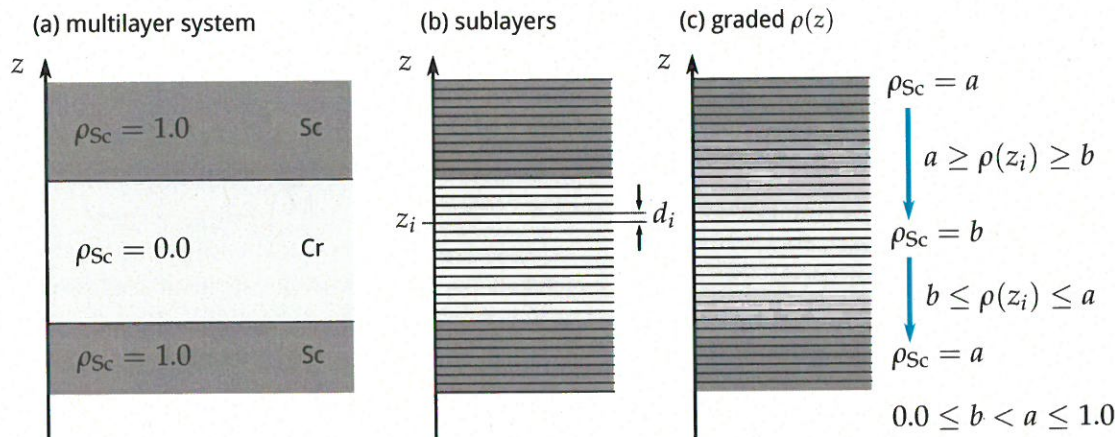


Figure 1.6 | Multilayer scheme to illustrate the method of calculating the x-ray fluorescence yield by the example of Sc in a Cr/Sc multilayer. The multilayer system (a) is split into multiple equidistant sub-layers (b) to obtain the field intensity at discrete points inside the Sc and Cr layers by applying the matrix algorithm in Sec. 1.3. The relative density of Sc ρ_{Sc} is multiplied by the respective intensity inside each sublayer. In case of a more a realistic intermixed system, the intensity is calculated similarly to (b) for discrete equidistant sub-layers. However, they differ by their relative Sc density, which is now generally different for each layer (c). In that case, it is possible that no pure Sc and Cr layers remain and thus $[\rho_{\text{Sc}}] < 1.0$ and $[\rho_{\text{Sc}}] > 0.0$, respectively.

integral thus turns into a discrete sum as

$$I_{\text{EKFRF}} = \tilde{C} \sum_i^M |E(z_i)|^2 \rho(z_i) d_i, \quad (1.53)$$

where M is the total number of sublayers of the whole stack.

In case of a theoretical multilayer system with perfectly sharp interfaces and no interdiffusion, the relative density of ρ_{Sc} in the given example will be binary, i.e. either $\rho_{\text{Sc}} = 1.0$ in the Sc (sub-)layers or $\rho_{\text{Sc}} = 0.0$ in the Cr layers. That, however, does not reflect a realistic situation, where interdiffusion of interface imperfections could lead to a mixture of the two materials in the sublayers. The third example in part (c) of Fig. 1.6 refers to a more realistic case, where the two materials interdiffuse with asymmetric interface regions. There, the relative Sc density ρ_{Sc} varies gradually from the highest value a to its lower value b . In general, a and b will not attain the values 1.0 and 0.0, respectively, as in the cases (a) and (b). That is, because the possibility exists that the two materials interdiffuse so strong, that no region with pure Sc or pure Cr remains.

* The necessary number of samples for a given system can be determined heuristically by evaluating the calculated fluorescence signal for an increasing number of sublayers until the numerical change of the result saturates.

The x-ray standing wave analysis of periodic multilayer systems

The section above covers the case of general multilayer systems. Here, we now shall consider the special case of strongly periodic layers [12, 14], such as multilayer mirror systems demonstrated by means of a specific example. Again, we consider a Cr/Sc multilayer system. If we choose the layer thicknesses to be $d_{\text{Sc}} = 0.6 \text{ nm}$ and $d_{\text{Cr}} = 0.7 \text{ nm}$ periodically replicated $N = 400$ times with perfectly sharp interfaces, i.e. the case (a) and (b) of Fig. 1.6, we obtain a one-dimensional artificial Bragg crystal. Radiation of 6.25 keV is well above the K-absorption edges of both materials and thus causes the emission of the K-line fluorescence radiation. For grazing angles of incidence between $\alpha_i^{\text{GI}} = 3.7^\circ$ and $\alpha_i^{\text{GI}} = 3.9^\circ$ and for this photon energy the reflected field amplitudes at each interface interfere constructively causing the appearance of the first order Bragg peak of the periodic layer structure. The corresponding calculation employing the matrix method from Sec. 1.3 is shown in Fig. 1.7(a).

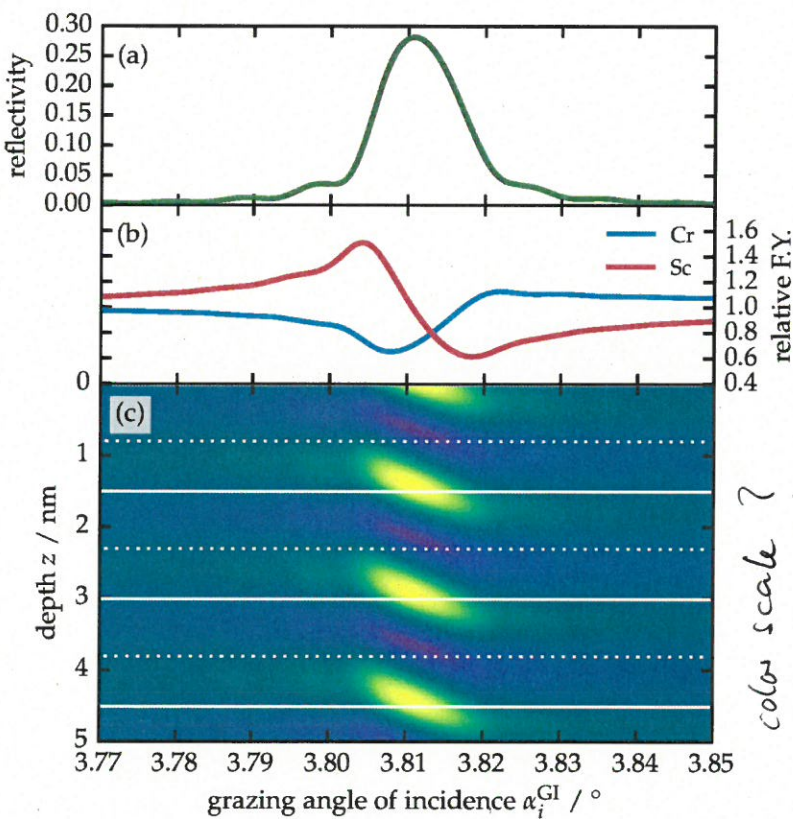


Figure 1.7 | Illustration of the grazing incidence X-ray standing wave fluorescence analysis. The exemplary system shown is a bilayer multilayer mirror of Cr and Sc irradiated with a 6.25 keV photon beam at grazing angles. Changing the grazing angle of incidence α_i^{GI} across the first Bragg peak (a) causes a standing wave inside the multilayer (total intensity in first top layers shown in (c)) and cause a relative fluorescence yield for the two different materials as shown in (b).

The constructive interference in the Bragg condition, in addition to resulting in a high reflectance, causes the formation of a X-ray standing wave inside the layers. The corresponding intensity distribution in the top first few layer pairs for the example given here is shown in Fig. 1.7(c). The standing wave intensity shifts through the individual layers thereby selectively exciting fluorescence radiation in the respective chemical species while changing the angle of incidence across the Bragg peak. Thus, this yields a method for chemically selective composition analysis with spatial resolution in the sub-nanometer regime called X-ray standing wave (XSW) analysis. The response curves of the respective relative fluorescence radiation intensity across the Bragg peak for both materials is shown in Fig. 1.7(b). In this example, the fluorescence radiation was calculated according to the discrete sum in Eq. (1.53) with a sublayer setup as indicated in Fig. 1.6(b) and 60

FUNDAMENTALS

sublayers per layer pair in each period.

The example above can be extended to the case of imperfect layer stacks with interdiffusion as discussed above. The corresponding calculation is then calculated according to the scheme given in Fig. 1.6(c).

→ reige Vergleich f= δ_{ab}

1.6 (b) und 1.6 (c)

⇒ Empfehlung von Fried →

References

- [1] J. Als-Nielsen and D. McMorrow: 'X-rays and their interaction with matter'. en. In: *Elements of Modern X-ray Physics*. John Wiley & Sons, Inc., 2011, pp. 1–28.
- [2] F. d. Bergevin: 'The Interaction of X-Rays (and Neutrons) with Matter'. en. In: *X-ray and Neutron Reflectivity*. Ed. by J. Daillant and A. Gibaud. Lecture Notes in Physics 770. DOI: [10.1007/978-3-540-88588-7_1](https://doi.org/10.1007/978-3-540-88588-7_1). Springer Berlin Heidelberg, 2009, pp. 1–57.
- [3] D. K. G. d. Boer, A. J. G. Leenaers and W. W. v. d. Hoogenhof: 'Influence of roughness profile on reflectivity and angle-dependent X-ray fluorescence'. In: *J. Phys. III France* 4.9 (1994), pp. 1559–1564. DOI: [10.1051/jp3:1994222](https://doi.org/10.1051/jp3:1994222).
- [4] D. K. G. de Boer: 'Glancing-incidence x-ray fluorescence of layered materials'. In: *Physical Review B* 44.2 (1991), pp. 498–511. DOI: [10.1103/PhysRevB.44.498](https://doi.org/10.1103/PhysRevB.44.498).
- [5] D. K. G. de Boer: 'X-ray reflection and transmission by rough surfaces'. In: *Phys. Rev. B* 51.8 (1995), pp. 5297–5305. DOI: [10.1103/PhysRevB.51.5297](https://doi.org/10.1103/PhysRevB.51.5297).
- [6] D. K. G. de Boer: 'X-ray scattering and x-ray fluorescence from materials with rough interfaces'. In: *Phys. Rev. B* 53.10 (1996), pp. 6048–6064. DOI: [10.1103/PhysRevB.53.6048](https://doi.org/10.1103/PhysRevB.53.6048).
- [7] M. Born and E. Wolf: *Principles of Optics*. 3rd ed. Cambridge University Press, 1965.
- [8] J. W. Criss and L. S. Birks: 'Calculation methods for fluorescent x-ray spectrometry. Empirical coefficients versus fundamental parameters'. In: *Analytical Chemistry* 40.7 (1968), pp. 1080–1086. DOI: [10.1021/ac60263a023](https://doi.org/10.1021/ac60263a023).
- [9] Croce, P. and Nérot, L.: 'Étude des couches minces et des surfaces par réflexion rasante, spéculaire ou diffuse, de rayons X'. In: *Rev. Phys. Appl. (Paris)* 11.1 (1976), pp. 113–125. DOI: [10.1051/rphysap:01976001101011300](https://doi.org/10.1051/rphysap:01976001101011300).
- [10] J. Daillant, S. Mora and A. Sentenac: 'Diffuse Scattering'. en. In: *X-ray and Neutron Reflectivity*. Ed. by J. Daillant and A. Gibaud. Lecture Notes in Physics 770. DOI: [10.1007/978-3-540-88588-7_4](https://doi.org/10.1007/978-3-540-88588-7_4). Springer Berlin Heidelberg, 2009, pp. 133–182.
- [11] J. Daillant, A. Gibaud, W. Beiglböck, J. Ehlers, K. Hepp, H. A. Weidenmüller, R. Beig, W. Domcke, B.-G. Englert, U. Frisch, P. Hänggi, G. Hasinger, W. Hillebrandt, R. L. Jaffe, W. Janke, H. v. Löhneysen, M. Mangano, J.-M. Raimond, D. Sornette, S. Theisen, W. Weise, J. Zittartz, F. Guinea and D. Vollhardt, eds.: *X-ray and Neutron Reflectivity*. Vol. 770. Lecture Notes in Physics. Berlin, Heidelberg: Springer Berlin Heidelberg, 2009.

References

- [12] B. N. Dev, A. K. Das, S. Dev, D. W. Schubert, M. Stamm and G. Materlik: 'Resonance enhancement of x rays in layered materials: Application to surface enrichment in polymer blends'. In: *Physical Review B* **61**.12 (2000), pp. 8462–8468. DOI: 10.1103/PhysRevB.61.8462.
- [13] P. a. M. Dirac: 'A new notation for quantum mechanics'. In: *Mathematical Proceedings of the Cambridge Philosophical Society* **35**.3 (1939), pp. 416–418. DOI: 10.1017/S0305004100021162.
- [14] S. K. Ghose and B. N. Dev: 'X-ray standing wave and reflectometric characterization of multilayer structures'. In: *Physical Review B* **63**.24 (2001), p. 245409. DOI: 10.1103/PhysRevB.63.245409.
- [15] A. Gibaud and G. Vignaud: 'Specular Reflectivity from Smooth and Rough Surfaces'. en. In: *X-ray and Neutron Reflectivity*. Ed. by J. Daillant and A. Gibaud. Lecture Notes in Physics 770. DOI: 10.1007/978-3-540-88588-7_3. Springer Berlin Heidelberg, 2009, pp. 85–131.
- [16] E. M. Gullikson and D. G. Stearns: 'Asymmetric extreme ultraviolet scattering from sputter-deposited multilayers'. In: *Phys. Rev. B* **59**.20 (1999), pp. 13273–13277. DOI: 10.1103/PhysRevB.59.13273.
- [17] A. Haase, S. Bajt, P. Hönicke, V. Soltwisch and F. Scholze: 'Multiparameter characterization of subnanometre Cr/Sc multilayers based on complementary measurements'. en. In: *Journal of Applied Crystallography* **49**.6 (2016), pp. 2161–2171. DOI: 10.1107/S1600576716015776.
- [18] A. Haase, V. Soltwisch, S. Braun, C. Laubis and F. Scholze: 'Interface Morphology of Mo/Si Multilayer Systems with Varying Mo Layer Thickness Studied by EUV Diffuse Scattering'. In: *Optics Express* (2017).
- [19] A. Haase, V. Soltwisch, C. Laubis and F. Scholze: 'Role of dynamic effects in the characterization of multilayers by means of power spectral density'. In: *Appl. Opt.* **53**.14 (2014), pp. 3019–3027. DOI: 10.1364/AO.53.003019.
- [20] A. Haase, V. Soltwisch, F. Scholze and S. Braun: 'Characterization of Mo/Si mirror interface roughness for different Mo layer thickness using resonant diffuse EUV scattering'. In: *Proc. SPIE*. Vol. 9628. 2015, pages. DOI: 10.1117/12.2191265.
- [21] V. Holý and T. Baumbach: 'Nonspecular X-ray reflection from rough multilayers'. In: *Phys. Rev. B* **49**.15 (1994), pp. 10668–10676. DOI: 10.1103/PhysRevB.49.10668.
- [22] V. Holý, J. Kuběna, I. Ohlidal, K. Lischka and W. Plotz: 'X-ray reflection from rough layered systems'. In: *Phys. Rev. B* **47**.23 (1993), pp. 15896–15903. DOI: 10.1103/PhysRevB.47.15896.
- [23] L. D. Landau and E.M. Lifshitz: *Electrodynamics of Continuous Media*. A Course of Theoretical Physics 8. Oxford, London, New York, Paris: Pergamon Press, 1960.
- [24] H. A. Lorentz: 'The theorem of Poynting concerning the energy in the electromagnetic field and two general propositions concerning the propagation of light'. In: *Amsterdamer Akademie der Wetenschappen* **4** (1896), p. 176.
- [25] P. Mikulík: 'X-ray reflectivity from planar and structured multilayers'. PhD thesis. Thèse de l'Université Joseph Fourier, 1997.
- [26] Nérot, L. and Croce, P.: 'Caractérisation des surfaces par réflexion rasante de rayons X. Application à l'étude du polissage de quelques verres silicates'. In: *Rev. Phys. Appl. (Paris)* **15**.3 (1980), pp. 761–779. DOI: 10.1051/rphysap:01980001503076100.

- [27] U. Pietsch, V. Holý and T. Baumbach: *High-Resolution X-Ray Scattering From Thin Films to Lateral Nanostructures*. Springer, 2004.
- [28] M. Prasciolu, A. Haase, F. Scholze, H. N. Chapman and S. Bajt: 'Extended asymmetric-cut multilayer X-ray gratings'. EN. In: *Optics Express* **23**.12 (2015), pp. 15195–15204. DOI: 10.1364/OE.23.015195.
- [29] S. D. Rasberry and K. F. J. Heinrich: 'Calibration for interelement effects in x-ray fluorescence analysis'. In: *Analytical Chemistry* **46**.1 (1974), pp. 81–89. DOI: 10.1021/ac60337a027.
- [30] R. M. Rousseau: 'Fundamental algorithm between concentration and intensity in XRF analysis 1—theory'. en. In: *X-Ray Spectrometry* **13**.3 (1984), pp. 115–120. DOI: 10.1002/xrs.1300130306.
- [31] J. Sherman: 'The theoretical derivation of fluorescent X-ray intensities from mixtures'. In: *Spectrochimica Acta* **7** (1955), pp. 283–306. DOI: 10.1016/0371-1951(55)80041-0.
- [32] T. Shiraiwa and N. Fujino: 'Theoretical Calculation of Fluorescent X-Ray Intensities in Fluorescent X-Ray Spectrochemical Analysis.' en. In: *Japanese Journal of Applied Physics* **5**.10 (1966), p. 886. DOI: 10.1143/JJAP.5.886.
- [33] S. K. Sinha, E. B. Sirota, S. Garoff and H. B. Stanley: 'X-ray and neutron scattering from rough surfaces'. In: *Phys. Rev. B* **38**.4 (1988), pp. 2297–2311. DOI: 10.1103/PhysRevB.38.2297.
- [34] V. Soltwisch, A. Haase, J. Wernecke, J. Probst, M. Schoengen, S. Burger, M. Krumrey and F. Scholze: 'Correlated diffuse x-ray scattering from periodically nanostructured surfaces'. In: *Physical Review B* **94**.3 (2016), p. 035419. DOI: 10.1103/PhysRevB.94.035419.
- [35] E. Spiller, D. Stearns and M. Krumrey: 'Multilayer X-ray mirrors: Interfacial roughness, scattering, and image quality'. In: *Journal of applied physics* **74**.1 (1993), pp. 107–118.
- [36] D. G. Stearns: 'X-ray scattering from interfacial roughness in multilayer structures'. In: *Journal of Applied Physics* **71**.9 (1992), pp. 4286–4298. DOI: 10.1063/1.350810.
- [37] A. C. Thompson and D. Vaughan, eds.: *X-ray Data Booklet*. Second. Lawrence Berkeley National Laboratory, University of California, 2001.
- [38] B. Vidal and P. Vincent: 'Metallic multilayers for x rays using classical thin-film theory'. en. In: *Applied Optics* **23**.11 (1984), p. 1794. DOI: 10.1364/AO.23.001794.

Erklärung

Es wurden bereits Teile der Dissertation veröffentlicht.

Liste der Veröffentlichungen, welche in die Dissertation eingeflossen sind:

- 1) A. Haase, V. Soltwisch, C. Laubis und F. Scholze: „Role of dynamic effects in the characterization of multilayers by means of power spectral density“. In: *Appl. Opt.* **53**.14 (2014), S. 3019–3027. DOI: 10.1364/AO.53.003019
- 2) A. Haase, V. Soltwisch, F. Scholze und S. Braun: „Characterization of Mo/Si mirror interface roughness for different Mo layer thickness using resonant diffuse EUV scattering“. In: *Proc. SPIE*. Bd. 9628. 2015, pages. DOI: 10.1117/12.2191265
- 3) A. Haase, S. Bajt, P. Hönigke, V. Soltwisch und F. Scholze: „Multiparameter characterization of subnanometre Cr/Sc multilayers based on complementary measurements“. en. In: *Journal of Applied Crystallography* **49**.6 (Dez. 2016), S. 2161–2171. DOI: 10.1107/S1600576716015776
- 4) A. Haase, V. Soltwisch, S. Braun, C. Laubis und F. Scholze: „Interface Morphology of Mo/Si Multilayer Systems with Varying Mo Layer Thickness Studied by EUV Diffuse Scattering“. In: *Optics Express* (2017)

Liste der Veröffentlichungen, welche nicht in die Dissertation eingeflossen sind:

- 1) M. Prasciolu, A. Haase, F. Scholze, H. N. Chapman und S. Bajt: „Extended asymmetric-cut multilayer X-ray gratings“. EN. In: *Optics Express* **23**.12 (Juni 2015), S. 15195–15204. DOI: 10.1364/OE.23.015195
- 2) V. Soltwisch, A. Haase, J. Wernecke, J. Probst, M. Schoengen, S. Burger, M. Krumrey und F. Scholze: „Correlated diffuse x-ray scattering from periodically nanostructured surfaces“. In: *Physical Review B* **94**.3 (Juli 2016), S. 035419. DOI: 10.1103/PhysRevB.94.035419

Ich habe an keiner anderen Hochschule oder Fakultät eine Promotionsabsicht eingereicht.

Berlin, den 9. Dezember 2016

Anton Haase

